ORIGINAL SCIENTIFIC PAPER

CROATICA CHEMICA ACTA

Croat. Chem. Acta **2026**, *99*(2), 215–229
Published online: November 10, 2026
DOI: 10.5562/cca4360

HKD 1926

Influence of Activation Chemistry on Surface Characteristics and Pb^{2+} Adsorption by Chayote-Derived Activated Carbon

Nikili K. Zhimo, Neilanuo Huozha, Daniel Kibami*

Dept. of Chemistry, Kohima Science College, Jotsoma, India

* Corresponding author's e-mail address: danielkibs80@yahoo.co.in

RECEIVED: June 7, 2026 ✶ REVISED: September 11, 2026 ✶ ACCEPTED: September 29, 2026

Abstract: Activated carbon was synthesized from chayote (*Sechium edule*) biomass using KOH, HNO_3, and $FeCl_3$ as chemical activating agents, and its performance for Pb^{2+} removal from aqueous solution was systematically investigated. The influence of activation chemistry on the structural and surface characteristics of the resulting carbons was examined using BET, SEM, FTIR, XRD, EDX, pH_{zpc}, and XPS analyses. Distinct variations in pore development and surface functionality were observed among the three activated carbons, reflecting the different effects of the activating agents. KOH activation produced the most favourable adsorbent, exhibiting the highest specific surface area (1103.57 $m^2\ g^{-1}$), a Langmuir maximum adsorption capacity of 57.811 mg g^{-1}, and Pb^{2+} removal efficiencies approaching 98%. Equilibrium data were best represented by the Langmuir model for KOH- and HNO_3-activated carbons, whereas the Freundlich model more adequately described the adsorption behaviour of the $FeCl_3$-activated carbon. Kinetic analysis showed that the pseudo-second-order model provided the closest fit to the experimental data, while the combined characterization results suggested that Pb^{2+} adsorption was governed by the combined influence of electrostatic interactions, oxygen-containing surface functional groups, and diffusion within the pore network. These findings demonstrate that the choice of activating agent strongly influences the adsorption behaviour of chayote-derived activated carbon, with KOH activation producing the most effective adsorbent under the experimental conditions investigated.

Keywords: chayote biomass, activated carbon, lead adsorption, activation chemistry, heavy metal remediation, aqueous treatment.

INTRODUCTION

DESPITE the well-established toxicity, persistence, and non-biodegradable nature of Pb^{2+} which unlike organic pollutants, does not break down in water and can remain in aquatic systems for extended periods, its removal from water is still predominantly evaluated based on adsorption capacity alone. However, adsorbents exhibiting comparable capacities frequently demonstrate different performances under realistic conditions. This variation arises not only from differences in experimental parameters, but also from the way adsorption mechanisms are interpreted. In many studies, Pb^{2+} uptake is primarily correlated with surface area and pore structure, whereas the contribution of surface functional groups and specific binding interactions remains less thoroughly explored. Consequently, achieving improved adsorption performance requires a more comprehensive understanding of the interaction between Pb^{2+} ions and active surface sites, particularly in the presence of competing ions.[1] Even at low concentrations, lead exposure can cause severe health problems, especially affecting the nervous system and kidneys.[2,3] Continuous release from industrial sources such as battery manufacturing, electroplating, and mining has contributed to its widespread presence in water bodies.[4] Its persistence and tendency to accumulate in living systems emphasize the need for effective treatment technologies. As a result, organizations such as the World Health Organization and the U.S. Environmental Protection Agency have established strict regulatory limits for lead in water,[5,6] increasing the demand for adsorption systems that can perform efficiently under dilute and chemically complex conditions.

This work is licensed under a Creative Commons Attribution 4.0 International License.

Various techniques, including chemical precipitation, ion exchange, membrane processes, and electrochemical treatment, have been developed for Pb^{2+} removal. Although these methods are effective under controlled conditions, they often involve high operational costs, sensitivity to water chemistry, and the generation of secondary waste requiring further treatment.[7,8] In contrast, adsorption has emerged as a more practical approach due to its simplicity, efficiency, and adaptability. The availability of low-cost adsorbents derived from natural materials, industrial by-products, and agricultural residues further enhances its applicability, particularly for large-scale systems.[9] Activated carbon remains one of the most widely studied adsorbents for heavy metal removal. Increasing evidence indicates that adsorption behaviour is strongly influenced by surface functional groups, pore accessibility, and the chemical nature of active sites.[10–12] This has driven interest in tailoring biomass-derived carbon materials through controlled modification. In this context, chayote (*Sechium edule*), an underutilized lignocellulosic biomass, presents potential as a precursor for activated carbon. Despite its availability and favorable composition, its application in heavy metal adsorption remains limited, offering scope for developing adsorbents with tailored properties. Chemical activation plays a key role in defining the properties of carbon materials. KOH activation promotes pore development and surface area, whereas HNO_3 treatment introduces oxygen-containing functional groups that enhance metal ion interactions $FeCl_3$ activation modifies the surface by introducing iron-associated sites, enabling additional adsorption pathways such as coordination or surface complexation.[13–16] These strategies therefore produce distinct surface environments rather than simply improving adsorption to varying extents.

In this study, chayote (*Sechium edule*)-derived activated carbons prepared via KOH, HNO_3, and $FeCl_3$ activation were evaluated for Pb^{2+} removal) with emphasis on linking adsorption behaviour to surface characteristics. It is hypothesized that activation chemistry defines distinct surface environments, thereby governing both adsorption capacity and mechanism.

MATERIALS AND METHODS

Chayote (*Sechium edule*) biomass (leaves, stems, and vines) was used as the precursor for the activated carbon preparation. Potassium hydroxide (KOH), nitric acid (HNO_3), ferric chloride ($FeCl_3$), and lead nitrate [$Pb(NO_3)_2$] of analytical grade were used as received. All solutions were prepared using deionized water.

Preparation of Activated Carbon

The collected chayote biomass (stem and leaves) was washed thoroughly with distilled water and dried in a laboratory drying oven at 105 °C for 24 h. The dried biomass was placed in a covered stainless-steel container and carbonized in a muffle furnace. The temperature was increased from room temperature to 450 °C at a heating rate of 10 °C min^{-1} and maintained at 450 °C for 3 h to produce biochar. The use of the covered stainless-steel container restricted direct exposure of the biomass to atmospheric oxygen during thermal treatment. After carbonization, the biochar was allowed to cool naturally to room temperature inside the furnace before chemical activation. The obtained biochar was separately impregnated with KOH, HNO_3, and $FeCl_3$ at a precursor-to-activator ratio of 1 : 4 (*w* / *w*). Each mixture was agitated at 150 rpm for 24 h at room temperature and subsequently dried at 105 °C. The dried impregnated materials were placed in the covered stainless-steel container and heated in the muffle furnace from room temperature to 600 °C at 10 °C min^{-1}, followed by a holding period of 1 h at 600 °C. After activation, the materials were allowed to cool naturally to room temperature inside the furnace before washing with distilled water until neutral pH was attained. The washed materials were again dried in a laboratory drying oven at 105 °C, ground, and sieved to obtain particles in the 100–150 µm range. The resulting carbons were designated as KAC, HAC, and FAC for the KOH-, HNO_3-, and $FeCl_3$-activated materials, respectively.

Preparation of Pb^{2+} Solutions

A stock solution of Pb^{2+} (1000 mg L^{-1}) was prepared by dissolving $Pb(NO_3)_2$ in deionized water and diluting to 1 L. Working solutions (10–100 mg L^{-1}) were prepared by appropriate dilution of the stock solution.

Characterization of Adsorbents

The specific surface area and pore characteristics were determined using BET analysis (Quantachrome, USA). Surface morphology was examined using SEM and XRD (JEOL JSM-6390LV), and functional groups were identified using FTIR (PerkinElmer Spectrum 100/Frontier IR). The point of zero charge (pH_{zpc}) was determined using the pH drift method. The structural properties of the materials were analysed using X-ray diffraction (XRD- Xpert Pro MPD, Malvern Panaylytical). Surface elemental composition and chemical states were investigated using X-ray photoelectron spectroscopy (XPS- ESCALAB Xi+ Thermo Scientific) performed before and after Pb^{2+} adsorption.

Batch Adsorption Experiments

Batch adsorption experiments were carried out in 500 mL Erlenmeyer flasks containing 250 mL of Pb^{2+} solution. The effects of initial Pb^{2+} concentration (10–100 mg L^{-1}), adsorbent dosage (0.1–1.0 g), contact time (5 min to 24 h), and solution pH (2–10) were investigated. The pH was

adjusted using 0.1 M HCl or 0.1 M NaOH. All experiments were conducted at 25 ± 2 °C with agitation at 150 rpm. At predetermined intervals, samples were withdrawn, filtered, and analysed using ICP-OES (PerkinElmer Avio 220 Max). All experiments were performed in triplicate, and the results are reported as mean ± standard deviation. The removal efficiency and adsorption capacity were calculated using:

$$\text{Removal } \% = \frac{c_i - c_f}{c_i} \cdot 100\ \%$$

$$q_e = \frac{c_i - c_e}{m} \cdot V$$

where, c_i = initial concentration of Pb^{2+} (mg L^{-1}), c_f = final concentration of Pb^{2+} after treatment (mg L^{-1}), c_e = equilibrium concentration of Pb^{2+} (mg L^{-1}), m = mass of adsorbent used (g), V = volume of the solution (L).

Isotherm and Kinetic Modelling

All isotherm and kinetic models were fitted using nonlinear regression in OriginPro 8.5 (OriginLab) to obtain the model parameters directly. The experimental data were fitted directly to the nonlinear forms of each model, and the resulting parameters were used for subsequent model evaluation. Parameter uncertainty and confidence interval analyses were not included in the present study.

The Langmuir model, which assumes monolayer adsorption on a homogeneous surface with identical active sites along with Separation factor R_L, is expressed as:

$$q_e = \frac{q_m K_L c_e}{1 + K_L c_e} \qquad R_L = \frac{1}{1 + K_L c_0} \tag{1}$$

where q_e - adsorption capacity at equilibrium (mg g^{-1}), q_m – max. monolayer adsorption capacity (mg g^{-1}), K_L -Langmuir adsorption constant (L mg^{-1}), c_e -equilibrium conc. of adsorbate in solution (mg L^{-1}).

The Freundlich model, describing adsorption on heterogeneous surfaces, is given by:

$$q_e = K_F (c_e)^{\frac{1}{n}} \tag{2}$$

where q_e - adsorption capacity at equilibrium (mg g^{-1}), K_F - adsorption capacity constant, n - adsorption intensity, c_e- equilibrium conc. of adsorbate in solution (mg L^{-1}).

The Temkin isotherm, which accounts for adsorbate–adsorbent interactions and variations in adsorption energy, is expressed as:

$$q_e = B\ \ln(A_T c_e) \tag{3}$$

where q_e - adsorption capacity at equilibrium (mg g^{-1}), B - heat of adsorption, A_T-Temkin equilibrium binding constant (L g^{-1}), c_e-equilibrium conc. of adsorbate in solution (mg L^{-1}).

All isotherm models were fitted using nonlinear regression to obtain model parameters directly. The adsorption kinetics of Pb^{2+} were analysed using pseudo-first-order and pseudo-second-order models, both applied in their nonlinear forms.

The pseudo-first-order model is expressed as

$$q_t = 1 - \exp^{-K_1 t} \tag{4}$$

where q_t - capacity at time t(min^{-1}) , q_e- adsorption capacity at equilibrium (mg g^{-1}), K_1 - (min^{-1}) is the rate constant.

The pseudo-second-order model is given by:

$$q_t = \frac{K_2 q_e^2 t}{1 + K_2 q_e t} \tag{5}$$

where q_t- capacity at time t, q_e- adsorption capacity at equilibrium (mg g^{-1}), K_2 - rate constant (g mg^{-1} min^{-1}).

To further investigate the adsorption mechanism, the intraparticle diffusion (IPD) model was applied and is expressed as:

$$q_t = K_d t^{\frac{1}{2}} + C \tag{6}$$

where q_t- capacity at time t (min), K_d - diffusion rate constant, C represents the boundary layer thickness.

The IPD plots were analysed for multi-linearity to distinguish between boundary layer diffusion and diffusion within the pores of the adsorbent. The suitability of the kinetic models was assessed based on the coefficient of determination (R^2) and the agreement between experimental and calculated equilibrium adsorption capacities (q_e).

Error Analysis

To evaluate the agreement between the experimental data and the adsorption models, chi-square (χ^2) and root mean square error (RMSE) were employed alongside the coefficient of determination (R^2). Although R^2 provides an indication of the overall goodness-of-fit, it does not adequately reflect the magnitude and distribution of deviations between the experimental observations and model predictions. Therefore, χ^2 and RMSE were used to quantify these deviations and provide a more comprehensive assessment of model performance. Models with lower χ^2 and RMSE

values were considered to better represent the experimental adsorption behaviour. The combined use of these statistical indicators with R^2 is widely adopted for evaluating nonlinear adsorption models.[23,24] The χ^2 and RMSE values were calculated by comparing the experimentally determined adsorption capacities with the corresponding values predicted by the nonlinear regression models. For the isotherm analysis, nonlinear regression was performed using ten equilibrium data points corresponding to initial Pb^{2+} concentrations ranging from 10 to 100 mg L^{-1}. In the error function equations, q_e and q_c represent the experimental and calculated adsorption capacities, respectively, while mmm denotes the total number of experimental data points included in each nonlinear regression analysis.

$$\chi^2 = \sum_{i=1}^{m}\left(\frac{q_e - q_c}{q_c}\right)^2 \quad (7)$$

$$RMSE = \sqrt{\frac{1}{m-2}\sum_{i=1}^{m}(q_e - q_c)^2} \quad (8)$$

Regeneration and Reusability Assessment

The regeneration and reusability of KAC, HAC, and FAC were assessed over five successive adsorption–desorption cycles. Following each adsorption cycle, the exhausted adsorbent was treated with 0.1 M NaOH solution to desorb the retained Pb^{2+} ions. The material was subsequently washed with distilled water until neutral pH was attained, then dried prior to reuse. The regenerated adsorbent was reapplied under identical experimental conditions in each subsequent cycle to evaluate its stability and reusability performance.

Comparison with Commercial Activated Carbon

For comparative evaluation, a commercially available powdered activated carbon (CAC) was used as a reference adsorbent. The commercial material was used as received without further chemical treatment and sieved to obtain a particle size of 100–150 µm, comparable to that of the synthesized activated carbons (Information regarding its specific surface area and pore characteristics was not available from the manufacturer and was therefore not determined in the present study). Adsorption experiments were performed under the same optimized conditions used for the synthesized activated carbons, using an initial Pb^{2+} concentration of 70 mg L^{-1}, an adsorbent dosage of 1.0 g, solution pH 6.0, a contact time of 24 h, agitation at 150 rpm, and a temperature of 25 ± 2 °C. Following adsorption, the suspensions were filtered and the residual Pb^{2+} concentration was determined using ICP-OES.

Adsorption in Spiked Natural Water Samples

The applicability of the synthesized activated carbons under more representative water conditions was investigated using Pb^{2+}-spiked natural water samples. Natural water was collected from Jotsoma Village (25.69215° N, 93.96780° E), Nagaland, in clean polyethylene containers and stored at room temperature until use. Prior to the adsorption experiments, the water was characterized for its physicochemical properties, including pH (7.3), electrical conductivity (5.81 µS cm^{-1}), total dissolved solids (3.82 mg L^{-1}), salinity (1.61 mg L^{-1}), total hardness (54 mg L^{-1}), calcium (12.02 mg L^{-1}), and magnesium (5.84 mg L^{-1}). The sample was subsequently spiked with Pb^{2+} to obtain an initial concentration of 70 mg L^{-1}. Batch adsorption experiments were carried out using 1 of adsorbent with a contact time of 24 h at 25 ± 2 °C and an agitation speed of 150 rpm**.** The natural water pH was maintained without further adjustment throughout the experiment. After adsorption, the suspensions were filtered and the residual Pb^{2+} concentration was quantified using ICP-OES (PerkinElmer Avio 220 Max). The adsorption performance obtained in the natural water matrix was compared with that observed in deionized water under identical experimental conditions.

RESULTS AND DISCUSSION

Surface Charge Characteristics (pH_{zpc})

The pH_{zpc} values (Figure 1) varied with the activating agent, highlighting the marked influence of chemical activation on the surface characteristics of the prepared carbons. KOH activation resulted in the highest pH_{zpc} (~6.5), whereas HNO_3- and $FeCl_3$-activated carbons exhibited lower values (~4–5), indicating a comparatively more acidic surface following oxidative activation.[25] Below the pH_{zpc}, the adsorbent surface carries a net positive charge, reducing its affinity for Pb^{2+} ions because of electrostatic repulsion. As the solution pH exceeds the pH_{zpc}, the surface becomes increasingly negatively charged, creating more favourable conditions for Pb^{2+} adsorption, although other interactions may also contribute to the overall adsorption process.[26,27].

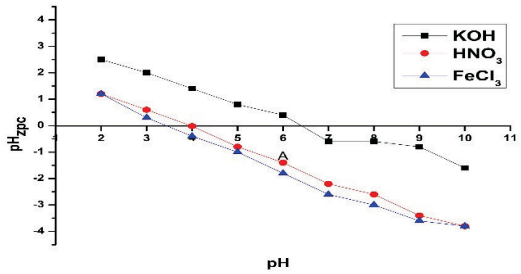


Figure 1. pH_{zpc} of KAC, HAC and FAC.

These differences in pH_{zpc} demonstrate that the choice of activating agent alters the surface charge characteristics of the carbon, thereby influencing its interaction with Pb^{2+} ions over different pH ranges.

Physicochemical and Textural Characterization

Activated carbons prepared at a 1 : 4 precursor-to-activator ratio exhibited clear differences in composition and pore structure depending on the activating agent (Table 1). KOH activation resulted in higher fixed carbon (79.60 %) and lower ash content, along with the highest iodine number (907.87 mg g^{-1}), suggesting enhanced microporosity.[24,25].

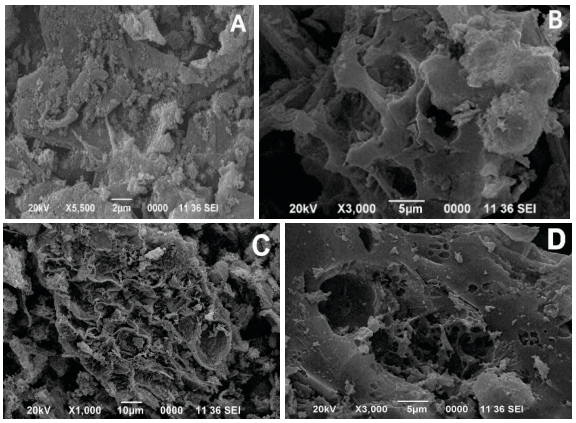


Figure 2. SEM images of (A) Unactivated Carbon, (B) KOH Activated Carbon, (C) HNO_3 Activated Carbon (D) $FeCl_3$ Activated Carbon.

In agreement with this, it also displayed the highest BET surface area (1103.57 m^2 g^{-1}) and pore volume (0.601 cm^3 g^{-1}), which are typical of effective KOH activation.[13] SEM images further reveal a well-developed and interconnected porous structure. HNO_3 activation yielded the highest recovery (34.01 %) with moderate structural development. Its BET surface area (925.71 m^2 g^{-1}) and iodine number (832.99 mg g^{-1}) indicate appreciable porosity, while SEM micrographs show a wrinkled and irregular surface. This suggests that oxidation mainly modifies surface characteristics rather than significantly enhancing pore formation, consistent with previous reports on nitric acid-treated carbons.[14,15] In contrast, $FeCl_3$ activation resulted in a lower surface area (756.94 m^2 g^{-1}), higher ash content, and reduced pore volume (0.403 cm^3 g^{-1}). SEM observations reveal irregular and partially obstructed structures, likely due to residual inorganic species, which may restrict pore accessibility and influence adsorption behaviour.[26,27]

Surface Functional Group Analysis (FTIR)

The FTIR spectra (Figure 3) confirm the presence of surface functional groups relevant to Pb^{2+} adsorption. A broad band at 3300–3500 cm^{-1} corresponds to O–H stretching, while peaks around 2850–3000 cm^{-1} are attributed to C–H vibrations, typical of carbon materials.[24,25] The KOH-activated carbon shows relatively weaker oxygen-related bands, with features near 1588 cm^{-1} (C=C) and 1287 cm^{-1} (C–O), indicating a more carbonized surface with limited functional groups. This suggests that adsorption is mainly

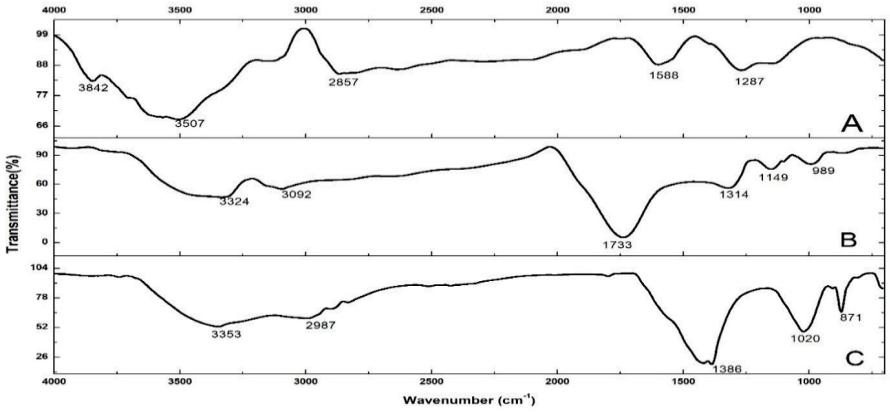


Figure 3. FTIR spectra of A- KOH AC, B- HNO_3 AC and C- $FeCl_3$ AC.

Table 1. Proximate and textural properties of activated carbons prepared at a 1:4 precursor-to-activator ratio.

Sample	Moisture / %	Ash / %	Volatile Matter / %	Fixed Carbon / %	Iodine / mg g^{-1}	BET Surface Area / m^2 g^{-1}	Pore Vol / cm^3 g^{-1}	Avg. Pore Diameter / nm
KAC (KOH)	2.40	2.10	11.91	79.60	907.87	1103.57	0.601	2.14
HAC (HNO_3)	4.08	2.92	14.73	66.78	832.99	925.71	0.489	2.11
FAC ($FeCl_3$)	4.50	3.11	19.11	66.19	708.49	756.94	0.403	2.13

governed by its developed pore structure [13]. In contrast, the HNO_3-treated carbon exhibits a distinct band at 1733 cm^{-1} (C=O) along with peaks between 1314 and 989 cm^{-1}, indicating the introduction of oxygen-containing groups that can enhance Pb^{2+} adsorption through surface interactions.[14,15] For the $FeCl_3$-activated carbon, bands at 1386, 1020, and 871 cm^{-1} are associated with C–O vibrations and possible metal–oxygen linkages, suggesting the presence of residual inorganic species that may influence adsorption behaviour.[27] Overall, KOH activation favours pore-driven adsorption, HNO_3 enhances surface functionality, and $FeCl_3$ shows a combined but comparatively moderate effect.

EDX and XRD Analysis

The XRD patterns (Figure 4) indicate that all synthesized activated carbons are predominantly amorphous, exhibiting broad diffraction features characteristic of disordered carbonaceous materials. KOH-activated carbon displayed slightly greater structural ordering than the HNO_3- and $FeCl_3$-activated samples, although all materials retained an essentially amorphous nature. Such structural characteristics are favourable for adsorption because they provide abundant defects and accessible adsorption sites.[26,27] The EDX analysis further demonstrated that the activating agent influenced the elemental composition of the synthesized activated carbons. Carbon and oxygen were the predominant elements in all samples, confirming the successful conversion of chayote biomass into activated carbon. KOH-activated carbon exhibited the highest carbon content and comparatively lower oxygen content, reflecting a greater degree of carbonization. In contrast, HNO_3 activation resulted in increased oxygen content, consistent with the formation of oxygen-containing surface functionalities observed in the FTIR spectra.[14,15] Fe was detected only in the $FeCl_3$-activated carbon, indicating the presence of residual iron-containing species following chemical activation. Together with its higher ash content and lower surface area, this suggests that $FeCl_3$ activation produced a comparatively more heterogeneous surface environment than KOH and HNO_3 activation [26,27]. However, because high-resolution Fe 2p XPS analysis was not performed, the chemical state and contribution of the detected Fe species to Pb^{2+} adsorption could not be conclusively established. Overall, the XRD and EDX results complement the BET and FTIR analyses, demonstrating that KOH activation primarily enhanced pore development, HNO_3 activation increased surface oxygen functionalities,

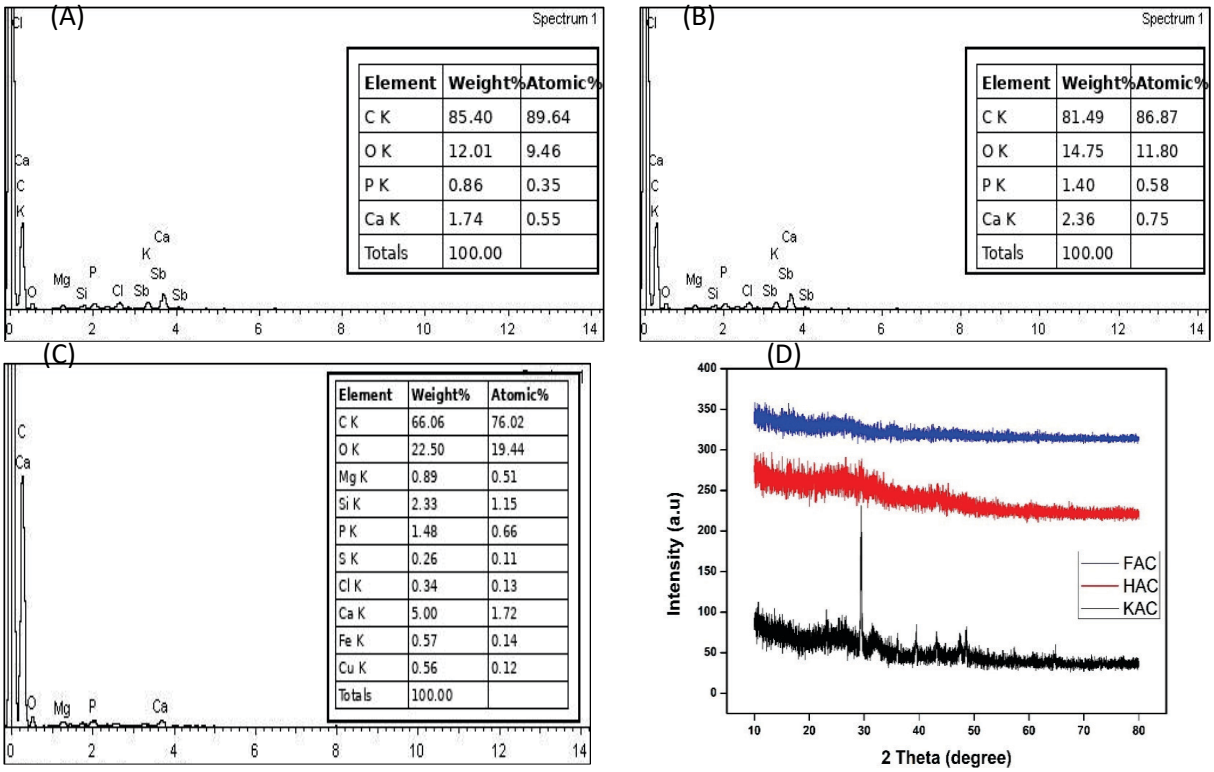


Figure 4. EDX spectra of KOH (A), HNO_3 (B), and $FeCl_3$(C) activated carbon samples showing the elemental composition of the prepared adsorbents and (D) XRD patterns of KOH, HNO_3, and $FeCl_3$ activated carbon samples showing the structural characteristics of the prepared adsorbents.

whereas $FeCl_3$ activation resulted in a more heterogeneous surface with detectable residual Fe. These differences are consistent with the observed adsorption performance of KOH-activated carbon > HNO_3-activated carbon > $FeCl_3$-activated carbon.[13–15,26,27].

XPS

The XPS survey spectra acquired before and after Pb^{2+} adsorption were analysed to evaluate changes in the surface chemical composition of the synthesized activated carbon. Before adsorption, the survey spectrum was dominated by carbon and oxygen, with nitrogen detected in comparatively lower amounts, reflecting the characteristic elemental composition of the prepared adsorbent. Following Pb^{2+} adsorption, the appearance of the Pb4f signal confirmed the presence of Pb-containing species on the activated carbon surface, providing direct evidence for the successful uptake of lead ions [31,32]. Although carbon and oxygen remained the predominant surface elements after adsorption, the emergence of the Pb4f signal clearly demonstrated the effective immobilisation of Pb^{2+} on the synthesized activated carbon. The high-resolution O1s spectrum was further examined to characterise the oxygen-containing surface functionalities that may participate in the adsorption process. Peak deconvolution revealed contributions corresponding to carbonyl (C=O) and hydroxyl/ether (C–O/C–OH) groups, which are commonly associated with activated carbon materials and are recognised as potential interaction sites for heavy metal ions.[33,34] These oxygen-containing functionalities, together with the complementary FTIR results, suggest that the adsorption of Pb^{2+} is facilitated through interactions with chemically active surface groups. However, comparative analysis of binding-energy shifts before and after adsorption was not performed. Therefore, the available XPS data are insufficient to establish the specific nature of the Pb^{2+}–surface interaction or to determine the adsorption mechanism conclusively. Consequently, the XPS results are interpreted as supporting the involvement of surface oxygen functionalities in Pb^{2+} adsorption rather than providing conclusive evidence of specific surface complexation. Collectively, the XPS findings complement the FTIR analysis by confirming the presence of Pb species on the activated carbon after adsorption while highlighting the abundance of oxygen-containing functional groups that may contribute to Pb^{2+} binding. Although additional high-resolution analyses would be required to establish the precise nature of the adsorbent–adsorbate interactions, the present results clearly demonstrate the successful adsorption of Pb^{2+} and further support the potential of the synthesized activated carbon as an effective adsorbent for the removal of lead from contaminated aqueous systems.[35].

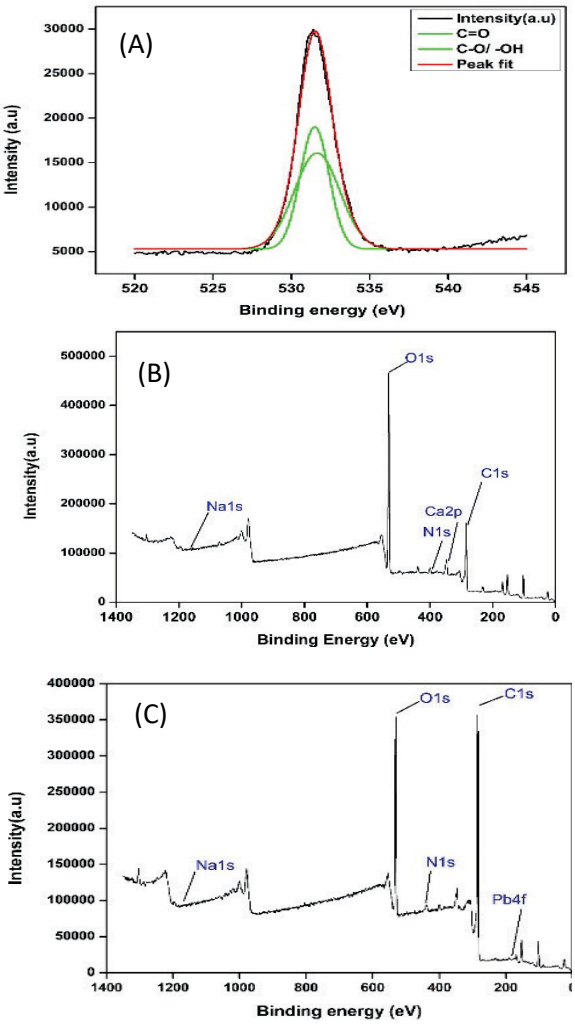


Figure 5. XPS characterization of the synthesized activated carbon before and after Pb^{2+} adsorption: (A) high-resolution O1s spectrum with peak fitting, (B) survey spectrum before adsorption, and (C) survey spectrum after adsorption.

Batch Adsorption

Based on the optimization studies described above, an initial Pb^{2+} concentration of 70 mg L^{-1}, adsorbent dosage of 1.0 g, solution pH of 5.0, contact time of 24 h, and a temperature of 25 ± 2 °C were selected for all subsequent adsorption experiments. These conditions were employed for the batch adsorption, isotherm, kinetic, regeneration, commercial activated carbon comparison, and natural water studies.

Effect of Initial Concentration and Dosage

The adsorption behaviour of the prepared activated carbons was significantly influenced by both the initial Pb^{2+}

concentration and adsorbent dosage. Increasing the Pb^{2+} concentration from 10 to 100 mg L^{-1} resulted in a gradual increase in adsorption capacity (q_e), indicating enhanced interaction between Pb^{2+} ions and the available adsorption sites. However, the overall removal efficiency decreased at higher concentrations due to progressive saturation of active sites. Among the prepared adsorbents, KOH-activated carbon exhibited the best performance, achieving a maximum removal efficiency of nearly 96 % along with the highest adsorption capacity. Similarly, increasing the adsorbent dosage from 0.2 to 1.0 g improved Pb^{2+} removal efficiency because of the greater availability of adsorption sites, whereas the adsorption capacity per unit mass decreased at higher dosages, likely due to partial particle aggregation and incomplete utilization of active sites. The superior adsorption performance of KOH-activated carbon can be attributed to its enhanced pore development and improved surface accessibility for Pb^{2+} adsorption.[28–30]

Effect of pH and Contact Time

The adsorption behaviour of the prepared activated carbons was strongly influenced by solution pH and contact time (Figure 7). Pb^{2+} removal increased steadily with increasing pH, reaching its highest value at pH 5 for all adsorbents. Under acidic conditions, the abundance of H^+ ions compete with Pb^{2+} for the available adsorption sites, resulting in lower removal efficiencies. A slight decrease in Pb^{2+} uptake beyond pH 5 suggests that changes in both the adsorbent surface charge and the aqueous speciation of lead begin to influence the adsorption process. As the solution becomes more alkaline, Pb^{2+} may undergo hydrolysis, and the possible formation of lead hydroxide species cannot be excluded. Therefore, Pb^{2+} removal at higher pH should not be interpreted solely as adsorption. Since the optimum adsorption was achieved at pH 5, all subsequent experiments were carried out under conditions where the contribution of precipitation is expected to be minimal. The pH-dependent adsorption behaviour also agrees well with the pH_{zpc} characteristics of the prepared adsorbents. The effect of contact time revealed a rapid initial uptake of Pb^{2+}, with more than 90 % removal achieved within the first 60 min, followed by a slower approach to equilibrium between 120 and 240 min as the remaining adsorption sites became progressively occupied. Among the prepared adsorbents, KOH activated carbon consistently exhibited the highest removal efficiency (~98 %) and adsorption capacity, reflecting its larger surface area and more developed pore structure as confirmed by the BET and SEM analyses.[28,30].

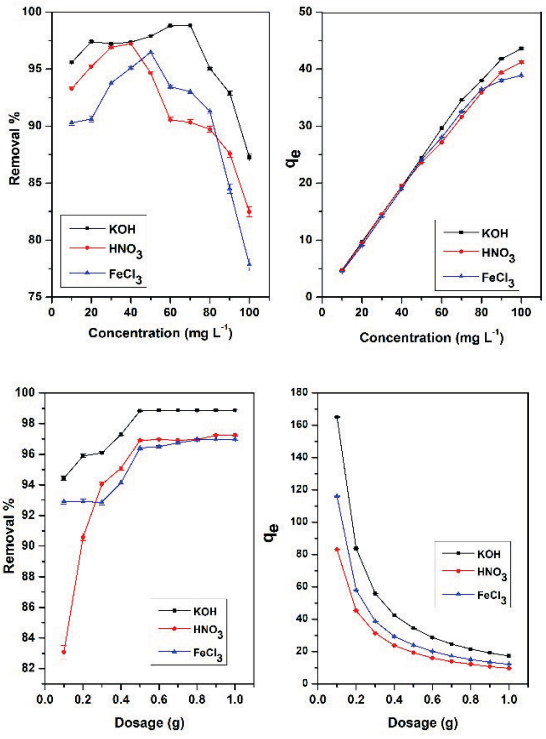


Figure 6. Influence of Pb^{2+} concentration and adsorbent dosage on the removal efficiency and adsorption capacity (q_e) of KOH-, HNO_3-, and $FeCl_3$-activated carbons.

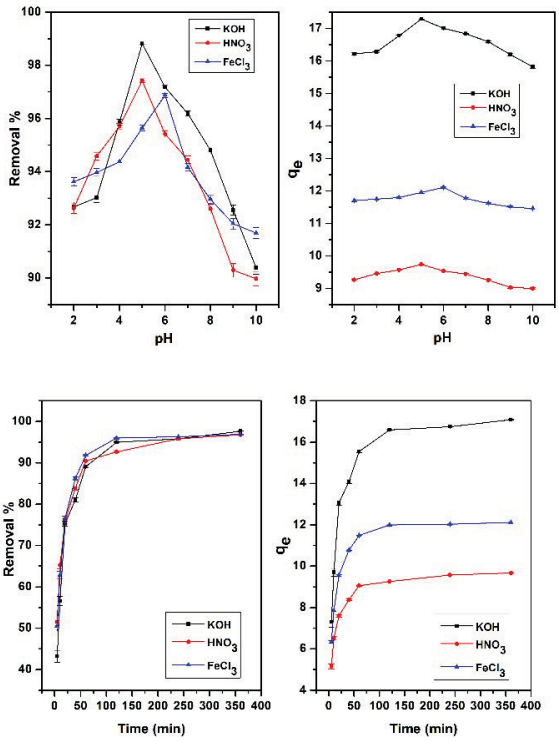


Figure 7. Influence of contact time and solution pH on the removal efficiency and adsorption capacity (q_t) of Pb^{2+} by KOH-, HNO_3-, and $FeCl_3$-activated carbons.

Adsorption Studies

ISOTHERM MODELLING

The equilibrium adsorption behaviour of Pb^{2+} onto the prepared activated carbons was examined using the Langmuir, Freundlich, and Temkin isotherm models (Figure 8 and Table 2). The Langmuir model showed the closest agreement with the equilibrium data for KOH- and HNO_3-activated carbons, as reflected by their higher R^2 values together with lower χ^2 and RMSE values. This indicates that Pb^{2+} adsorption on these adsorbents occurred predominantly through monolayer coverage on relatively homogeneous adsorption sites. The maximum monolayer adsorption capacities were estimated to be 57.811, 48.380, and 46.781 mg g^{-1} for KOH-, HNO_3-, and $FeCl_3$-activated carbons, respectively, following the same adsorption trend observed in the batch experiments. The equilibrium data obtained within the investigated concentration range (10–100 mg L^{-1}) were well described by the Langmuir model, providing reliable estimates of the adsorption parameters. The superior adsorption performance of KOH-activated carbon is attributed to its larger specific surface area, enhanced pore development, and greater accessibility of active sites, as evidenced by the BET and SEM analyses. Furthermore, the R_L values, which ranged between 0 and 1, confirmed that Pb^{2+} adsorption was favourable across the concentration range investigated. In comparison, the Freundlich model provided a better description of the adsorption behaviour of $FeCl_3$-activated carbon, suggesting a more heterogeneous surface with adsorption sites of varying energies. This observation is consistent with the surface characteristics revealed by the SEM, EDX, and XRD analyses, which indicated a less uniform pore structure and the presence of residual inorganic species following $FeCl_3$ activation. Likewise, the n^{-1} values below unity further support favourable adsorption for all prepared adsorbents. Although the Temkin model also described the equilibrium data, its comparatively lower fitting accuracy indicates that variations in adsorption energy alone could not fully account for the observed adsorption behaviour. Overall,

Table 2. Isotherm parameters and error analysis for Pb^{2+} adsorption onto KOH, HNO_3, and $FeCl_3$ activated carbons.

Model	Parameter	KAC	HAC	FAC
LANGMUIR	R^2	0.997	0.999	0.994
	q_{max} / mg g^{-1}	57.811	48.380	46.781
	K_L / L mg^{-1}	0.002	0.002	0.003
	R_L (dimensionless)	0.877	0.850	0.800
	χ^2	0.847	0.338	1.767
	RMSE / mg g^{-1}	0.920	0.581	1.329
FREUNDLICH	R^2	0.996	0.998	0.982
	K_F / mg g^{-1}	0.663	0.699	0.8199
	n^{-1}(dimensionless)	0.911	0.883	0.838
	χ^2	1.275	0.657	0.109
	RMSE / mg g^{-1}	1.129	0.811	0.331
TEMKIN	R^2	0.966	0.969	0.972
	A_T / L g^{-1}	0.093	0.088	0.093
	B / J mol^{-1}	18.016	17.425	16.719
	χ^2	14.042	7.132	5.950
	RMSE / mg g^{-1}	3.747	2.670	2.439

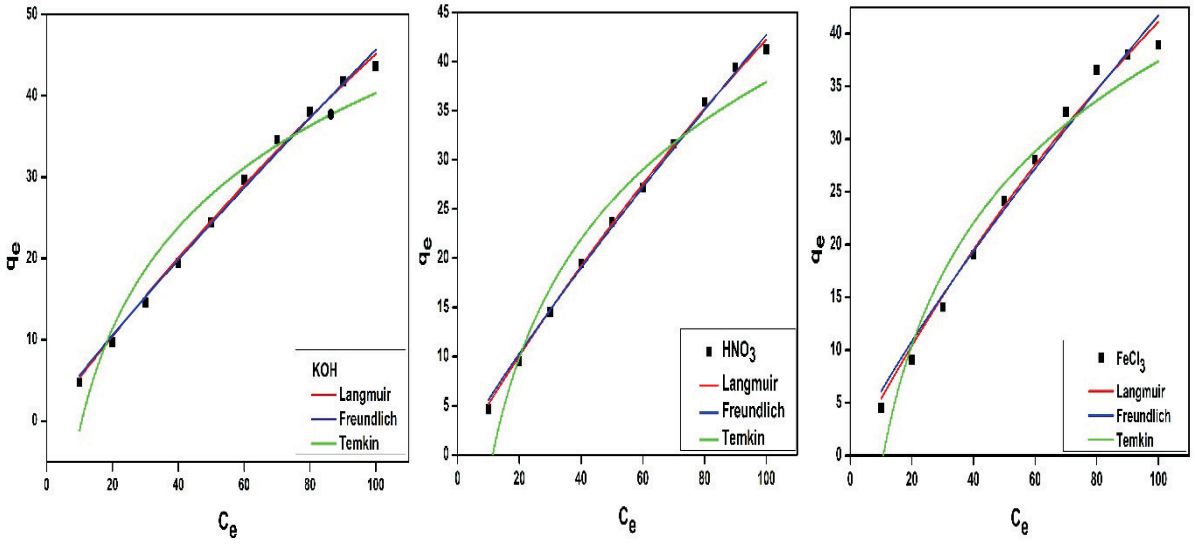


Figure 8. Langmuir, Freundlich, and Temkin isotherm model fitting for Pb^{2+} adsorption onto KOH, HNO_3, and $FeCl_3$ activated carbons.

the isotherm analysis demonstrates that activation chemistry had a pronounced influence on the adsorption characteristics of the prepared carbons, with KOH- and HNO_3-activated samples exhibiting predominantly monolayer adsorption, while $FeCl_3$ activation produced a comparatively more heterogeneous adsorption surface.[27,30].

KINETIC MODELLING

Pseudo First and Pseudo Second Order

The adsorption kinetics of Pb^{2+} onto the prepared activated carbons were analysed using the pseudo-first-order (PFO) and pseudo-second-order (PSO) models (Figure 9 and Table 3). Among the two models, the PSO model exhibited consistently better agreement with the experimental data, as reflected by higher R^2 values (0.99233–0.99652) together with lower χ^2 and RMSE values. Moreover, the calculated equilibrium adsorption capacities (q_{cal}) were in close agreement with the experimental values (q_{exp}), indicating that the PSO model more accurately represented the adsorption kinetics. Although the PFO model described the initial uptake reasonably well, its comparatively lower R^2 values and higher fitting errors suggest that it was less suitable for representing the overall adsorption process. Similar observations have been reported for Pb^{2+} adsorption onto biomass-derived activated carbons, where the PSO model consistently provides a better fit to the experimental data.[21–24,30–33] Among the prepared adsorbents, the KOH-activated carbon exhibited the highest equilibrium adsorption capacity (17.30 mg g^{-1}), which is consistent with its larger specific surface area and well-developed pore structure revealed by the BET and SEM analyses. The equilibrium adsorption capacities obtained from the kinetic study were lower than the Langmuir maximum adsorption capacities ($q$max), reflecting the different objectives of the two models rather than any inconsistency in the results. The kinetic experiments were performed at a fixed initial Pb^{2+} concentration (70 mg L^{-1}), whereas the Langmuir model was derived from equilibrium data collected over a broader concentration range (10–100 mg L^{-1}). Accordingly, the kinetic q_e values represent adsorption under a fixed experimental condition, whereas the Langmuir q_{max} corresponds to the theoretical maximum monolayer adsorption capacity obtained from equilibrium modelling.

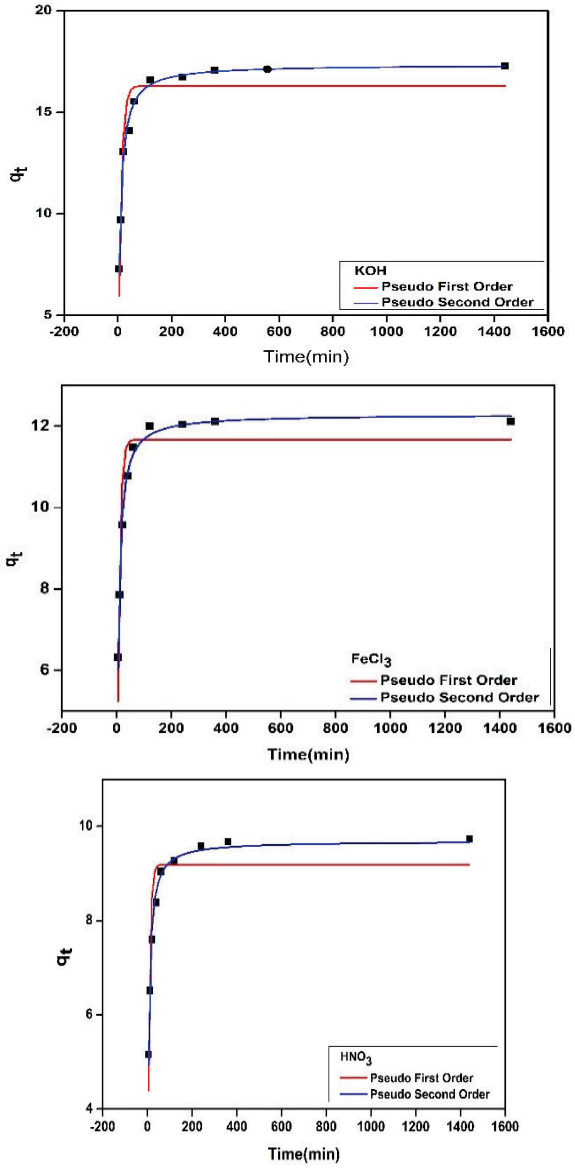


Figure 9. Kinetic parameters and fitting error analysis for Pb^{2+} adsorption onto KOH-, HNO_3-, and $FeCl_3$-activated carbons using pseudo-first-order, pseudo-second-order.

Table 3. Kinetic parameters and fitting error analysis for Pb^{2+} adsorption onto KOH-, HNO_3-, and $FeCl_3$-activated carbons using pseudo-first-order, pseudo-second-order.

Model	Parameter	KOH	HNO_3	$FeCl_3$
Pseudo First Order	R^2	0.961	0.931	0.886
	K_1 / min^{-1}	0.091	0.130	0.119
	q_{exp} / mg g^{-1}	17.297	9.728	12.116
	q_{cal} / mg g^{-1}	16.308	9.190	11.669
	χ^2 / mg g^{-1}	1.047	0.387	0.513
	RMSE / mg g^{-1}	1.047	0.622	0.716
Pseudo Second Order	R^2	0.996	0.995	0.992
	K_2 / min^{-1}	0.007	0.021	0.015
	q_{exp} / mg g^{-1}	17.297	9.728	12.116
	q_{cal} / mg g^{-1}	17.357	9.687	12.289
	χ^2 / mg g^{-1}	0.100	0.028	0.039
	RMSE / mg g^{-1}	0.316	0.168	0.199

Intra Particle Diffusion

The IPD plots exhibited clear multilinear behaviour, indicating that Pb^{2+} uptake did not proceed through a single diffusion pathway but involved successive mass-transfer stages. Accordingly, the q_t vs $t^{1/2}$ plots were divided into two linear regions, and each region was analysed independently (Figure 10 and Table 4). The steeper slopes observed in the initial region reflect the rapid uptake of Pb^{2+} immediately after contact with the adsorbents, when a large proportion of the surface adsorption sites remained readily available.[34]. Among the prepared activated carbons, KOH-activated carbon exhibited the highest diffusion rate constant (K_d), consistent with its larger BET surface area and more developed pore structure, which likely facilitated faster access to available adsorption sites [35,36] during the early stage of adsorption. As adsorption progressed, the slope decreased markedly in the second linear region, suggesting that the uptake rate became progressively slower as Pb^{2+} ions diffused into the internal pore network and the readily accessible surface sites were gradually occupied. The positive intercept (CCC) values obtained for both regions indicate that the fitted lines did not pass through the origin, demonstrating that intraparticle diffusion alone could not account for the adsorption kinetics. Instead, boundary-layer diffusion and external mass transfer also contributed throughout the adsorption process.[34,37,38] Overall, the multilinear IPD profiles suggest that Pb^{2+} adsorption involved a combination of transport mechanisms, beginning with rapid surface adsorption followed by slower pore diffusion. Although intraparticle diffusion contributed to Pb^{2+} uptake, the positive intercepts confirm that it was not the sole rate-controlling step, highlighting the simultaneous contribution of external mass transfer during the adsorption process.

Table 4. Intra-particle diffusion parameters obtained from separate linear regression of Region I and Region II for Pb^{2+} adsorption onto the prepared activated carbons.

Adsorbent	Region	$t^{1/2}$ / $min^{1/2}$	K_d / mg g^{-1} min^{-1}	C / mg g^{-1}	R^2
KOH	I	2.236–7.746	1.4282	5.1045	0.9148
	II	10.954–18.974	0.0601	15.8995	0.9176
HNO_3	I	2.236–7.746	0.6621	4.1722	0.9378
	II	10.954–18.974	0.0523	8.7176	0.9501
$FeCl_3$	I	2.236–7.746	0.9127	4.8305	0.9464
	II	10.954–18.974	0.0144	11.8339	0.9343

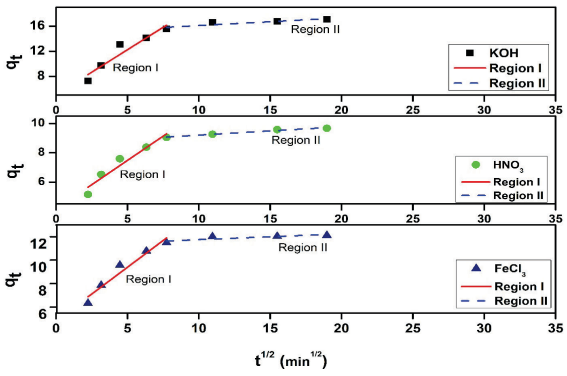


Figure 10. Intra-particle diffusion plots for Pb^{2+} adsorption onto (a) KOH-, (b) HNO_3-, and (c) $FeCl_3$-activated carbons, showing the independently fitted linear regions (Region I and Region II).

Adsorption Mechanism

Pb^{2+} adsorption by the synthesized activated carbons is more appropriately viewed as the combined effect of surface chemistry, surface charge, and pore structure rather than as the result of a single adsorption pathway. The differences observed among KAC, HAC, and FAC indicate that the choice of activating agent influenced the physicochemical properties of the resulting carbons and, consequently, their interaction with Pb^{2+}. The pH_{zpc} results suggest that electrostatic attraction contributed to Pb^{2+} uptake when the solution pH was above the pH_{zpc}, where the adsorbent surface would be expected to carry a greater negative charge. The lower adsorption under more acidic conditions can, in turn, be associated with competition from H^+ ions for available surface sites, which is consistent with the improved removal observed around pH 5–6.[25,26,28]. Thus, the pH-dependent behaviour supports a contribution from electrostatic interactions, although it does not establish electrostatic attraction as the sole mode of adsorption. The surface functional groups provide another important aspect of the adsorption behaviour. The FTIR spectra showed oxygen-containing functionalities, including hydroxyl, carbonyl, and C–O groups, that could serve as sites for Pb^{2+} interaction. The XPS results further showed the presence of Pb 4f signals following adsorption, confirming the retention of Pb-containing species on the carbon surface. However, the available XPS data do not provide sufficient evidence to distinguish conclusively between the possible modes of Pb^{2+} binding. The EDX results also revealed differences in the elemental composition of the activated carbons, reflecting changes in surface composition following the different activation treatments. When considered together with the SEM observations, which showed irregular surfaces containing cavities and channels, these results indicate that chemical activation altered both the surface morphology and the chemical environment of the carbons. The oxygen-containing functionalities appear to have contributed to Pb^{2+} uptake, although their individual contribution cannot be separated from the effects of pore structure and surface charge.[14,15,28,32,39].

The textural properties provide a further basis for understanding the higher adsorption exhibited by KAC. Among the three materials, KAC possessed the highest BET surface area (1103.57 m^2 g^{-1}), total pore volume (0.601 cm^3 g^{-1}), and iodine number (907.87 mg g^{-1}). Its comparatively developed surface structure, also evident from the SEM observations, would provide greater accessibility to adsorption sites than the lower-surface-area HAC and FAC. This greater availability of accessible surface may have facilitated Pb^{2+} transport into the porous carbon matrix and contributed to the higher uptake observed for KAC.[13,29–31,40] The kinetic behaviour is consistent with this interpretation. Although the pseudo-second-order model provided the best fit to the experimental data, the multilinear nature of the intraparticle-diffusion plots indicates that Pb^{2+} uptake did not proceed through a single transport step. The kinetic results therefore point to the involvement of successive processes, including surface interaction and diffusion within the porous structure, rather than providing direct evidence of a specific chemisorption mechanism.[21,22,33].

Overall, the higher Pb^{2+} adsorption capacity of KAC is consistent with the combined influence of its well-developed pore structure, favourable surface-charge characteristics, and chemically active surface functionalities. The results therefore do not support attributing the superior performance of KAC to any single surface property. Instead, the enhanced adsorption appears to arise from the way in which the physical and chemical characteristics developed during KOH activation collectively increased the availability and accessibility of sites for Pb^{2+} uptake under the conditions investigated.[13–15,28–32,39,40].

Regeneration and Reusability

The regeneration behaviour of the prepared activated carbons was assessed over five consecutive adsorption–desorption cycles to examine their potential for repeated Pb^{2+} removal (Figure 11). A gradual decrease in removal efficiency was observed for all three adsorbents with successive regeneration cycles, indicating that the adsorption performance could not be fully restored after each desorption step. Similar trends have been reported for biomass-derived activated carbons, where repeated use may lead to incomplete desorption of adsorbed metal ions together with gradual blockage or deactivation of accessible adsorption sites [30,33]. Among the synthesized adsorbents, KOH-activated carbon showed the highest regeneration stability, retaining more than 63 % of its initial Pb^{2+} removal efficiency after the fifth cycle, whereas HNO_3- and $FeCl_3$-activated carbons retained approximately 58 % and 52 %, respectively. The comparatively better performance of KOH-activated carbon is consistent with its higher surface area and more developed pore structure, which likely allowed greater accessibility to adsorption sites during repeated adsorption–desorption cycles.[13,28] Although the adsorbents remained reusable after five cycles, the progressive reduction in removal efficiency indicates that the regeneration procedure did not completely restore the original adsorption capacity. Because desorption efficiency and adsorbent mass recovery were not determined, the relative contribution of incomplete Pb^{2+} desorption, loss of adsorbent during handling, or possible changes in the adsorbent structure could not be established. Nevertheless, the results demonstrate that the synthesized activated carbons, particularly KOH-activated carbon, retained appreciable adsorption performance after repeated use, while also indicating that further optimization of regeneration conditions would be beneficial for long-term practical applications.

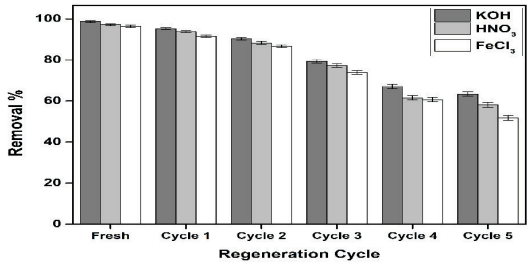


Figure 11. Regeneration and reusability performance of KOH-, HNO_3-, and $FeCl_3$-activated carbons during five consecutive Pb^{2+} adsorption–desorption cycles.

Comparison with commercial Carbon

The adsorption performance of the synthesized activated carbons was compared with that of a commercially available powdered activated carbon (CAC) under the same experimental conditions (Figure 12). All three synthesized carbons showed higher Pb^{2+} removal than the commercial material, with KAC giving the highest removal efficiency among the adsorbents tested. The comparatively better performance of the synthesized carbons may be related to the changes in pore structure and surface chemistry introduced during chemical activation, which provided

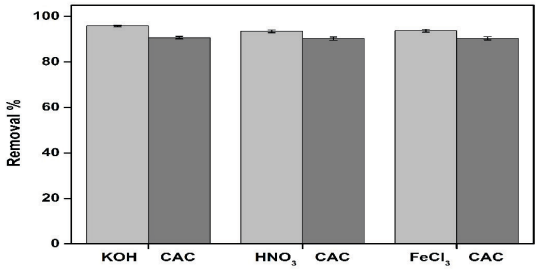


Figure 12. Comparison of Pb^{2+} removal efficiencies of the synthesized activated carbons with commercial activated carbon (CAC) under identical optimized adsorption conditions.

favourable conditions for Pb^{2+} uptake [13–15]. However, this comparison needs to be considered in the context of the available characterization data. The commercial activated carbon was not subjected to the same detailed physicochemical characterization, and information on properties such as specific surface area and pore characteristics was therefore unavailable. The difference in adsorption performance cannot, consequently, be linked solely to the type of activating agent or to differences in individual surface properties. The commercial carbon was included primarily as a practical benchmark to assess the performance of the prepared adsorbents under comparable experimental conditions, rather than for a direct material-to-material comparison of their physicochemical characteristics. Within this context, the results indicate that the chayote-derived activated carbons, particularly KAC, provide a competitive alternative for Pb^{2+} removal from aqueous solution.[28,30].

Adsorption in Spiked Natural Water Sample

To evaluate the applicability of the synthesized activated carbons under more representative water conditions, adsorption experiments were carried out using Pb^{2+}-spiked natural water collected from Jotsoma Village under the optimized adsorption conditions. The water sample had a pH of 7.3, total hardness of 54 mg L^{-1}, and contained Ca^{2+} (12.02 mg L^{-1}) and Mg^{2+} (5.84 mg L^{-1}), providing a more chemically complex matrix than deionized water. As shown in Figure 13, all three adsorbents maintained high Pb^{2+} removal efficiencies in the natural water sample, although a slight reduction compared with deionized water was observed. KAC exhibited the highest removal efficiency (~96 %), followed by HAC (~91 %) and FAC (~90 %). The decrease in adsorption performance is most likely related

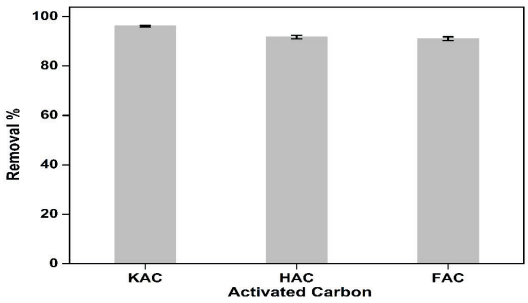


Figure 13. Pb^{2+} removal efficiency of KOH- (KAC), HNO_3- (HAC), and $FeCl_3$-activated (FAC) carbons in Pb^{2+}-spiked natural water under optimized adsorption conditions.

to the presence of naturally occurring ions, particularly Ca^{2+} and Mg^{2+}, which can compete with Pb^{2+} for the available adsorption sites.[30,40] Natural water may also contain other dissolved constituents capable of influencing Pb^{2+} uptake. Although dissolved organic matter was not analysed in the present study, its possible presence could also affect adsorption by interacting with Pb^{2+} ions or the adsorbent surface.[30,40] Despite these additional complexities, the synthesized activated carbons maintained high Pb^{2+} removal efficiencies, with KAC consistently exhibiting the best performance. These findings suggest that the prepared adsorbents remain effective under conditions that more closely resemble natural water than deionized laboratory solutions.

Comparison of Pb^{2+} Adsorption Performance with Reported Adsorbents

The adsorption capacities of the synthesized activated carbons were compared with those reported for biomass-derived adsorbents used for Pb^{2+} removal (Table 5). As adsorption performance is influenced by factors such as

Table 5. Comparison of Pb^{2+} adsorption capacities of the synthesized activated carbons with previously reported biomass-derived adsorbents.

Adsorbent precursor	Activation / Modification	Targeted heavy metal(s)	q_{max} / mg g^{-1}	Isotherm model	Reference
Apricot stone activated carbon	H_2SO_4 activation	Pb^{2+}	21.38	Langmuir	41
Banana peel activated carbon	KOH activation	Pb^{2+}, Cu^{2+}, Ni^{2+}	34.5 (Pb^{2+})	Langmuir	42
Banana peel activated carbon	Al_2O_3–chitosan modified	Pb^{2+}, Cd^{2+}	57.1 (Pb^{2+})	Freundlich	43
Rice husk ash	Thermal treatment / ash-derived adsorbent	Pb^{2+}	91.74	Freundlich	44
Magnetic coconut biochar	Fe-modified biochar	Pb^{2+}	153.1	Langmuir	28
Chayote AC (FAC)	$FeCl_3$ activation	Pb^{2+}	46.781	Freundlich	This study
Cherry kernel activated carbon	H_3PO_4 activation	Pb^{2+}, Cd^{2+}, Ni^{2+}	180.3 (Pb^{2+})	Langmuir	45
Chayote AC (HAC)	HNO_3 activation	Pb^{2+}	48.380	Langmuir	This study
Chayote AC (KAC)	KOH activation	Pb^{2+}	57.811	Langmuir	This study

solution pH, initial metal concentration, temperature, adsorbent dosage, and other experimental conditions, the reported values are intended to provide a general comparison rather than a direct ranking of adsorbents. Among the synthesized materials, KOH-activated carbon (KAC) exhibited the highest Langmuir maximum adsorption capacity (57.811 mg g^{-1}), followed by HNO_3-activated carbon (48.380 mg g^{-1}) and $FeCl_3$-activated carbon (46.781 mg g^{-1}). While the adsorption capacities of the synthesized activated carbons were lower than those reported for some highly modified biomass-derived adsorbents, they were comparable to several agricultural waste-based adsorbents reported in the literature. The superior performance of KAC can be attributed to its larger specific surface area, higher pore volume, and well-developed porous structure, which enhanced the accessibility of adsorption sites for Pb^{2+} uptake. These findings demonstrate that chayote-derived activated carbons are effective biomass-based adsorbents for Pb^{2+} removal and further highlight the important role of activation chemistry in tailoring their adsorption performance

CONCLUSION

Activated carbons were successfully prepared from *Sechium edule* biomass using KOH, HNO_3, and $FeCl_3$ as activating agents, producing materials with distinct physicochemical properties and Pb^{2+} adsorption behaviour. Among the prepared carbons, KOH-activated carbon showed the highest overall adsorption performance, with a Langmuir maximum adsorption capacity of 57.811 mg g^{-1}, along with higher Pb^{2+} removal and better retention of adsorption performance during regeneration. This performance is consistent with its higher specific surface area, greater pore volume, and more developed porous structure, which may have increased the accessibility of adsorption sites. HNO_3 activation, in comparison, favoured the development of oxygen-containing surface groups, while $FeCl_3$ activation produced a comparatively heterogeneous surface and lower Pb^{2+} uptake. The equilibrium data were best described by the Langmuir model for KOH- and HNO_3-activated carbons, whereas the pseudo-second-order model provided the closest fit to the kinetic data. Taken together, the characterization and adsorption results suggest that Pb^{2+} uptake involved the combined contribution of surface charge, oxygen-containing functional groups, accessible pore structure, and diffusion rather than a single adsorption pathway. Although the prepared carbons showed encouraging Pb^{2+} removal from spiked natural water, the study was conducted using a limited water matrix, and adsorption efficiency decreased progressively over repeated regeneration cycles. These results indicate the practical potential of the chayote-derived carbons, particularly KAC, for Pb^{2+} removal; however, their suitability for larger-scale treatment remains to be established. Further work should therefore examine their performance in continuous-flow systems, assess regeneration over a greater number of cycles, and evaluate their behaviour in real wastewater containing competing ions and other dissolved constituents. Such validation will be important for determining whether the adsorption performance observed under controlled laboratory conditions can be maintained in more complex treatment environments. Overall, the findings indicate that the choice of activating agent strongly influences the structural and surface characteristics of chayote-derived activated carbon, with KOH activation providing the most favourable combination of properties for Pb^{2+} removal under the conditions investigated.

Acknowledgment. The authors acknowledge the financial assistance from the National Fellowship for Scheduled Tribes (NFST), Government of India. Awardee no- 202122-NFST-NAG-01023(Nikili K Zhimo) and Awardee no- 202122-NFST-NAG- 010120 (Neilanuo Huozha). The authors gratefully acknowledge the Department of Chemical Sciences and the Sophisticated Analytical Instrumentation Facility (SAIF), Tezpur University, Assam, IIT Ropar Central Research Facility (CRF) for their for providing instrumental support and the Department of Chemistry, Kohima Science College, Nagaland, for providing research facilities and support during the course of this study.

REFERENCES

[1] Q. Shi, G. E. Sterbinsky, V. Prigiobbe, X. Meng, *Langmuir* **2018**, *34*, 13565–13573. https://doi.org/10.1021/acs.langmuir.8b03096

[2] A. M. Badran, U. Utra, N. S. Yussof, M. J. Bashir, *Separations* **2023**, *10*, 565. https://doi.org/10.3390/separations10110565

[3] A. Ara, J. A. Usmani, *Interdiscip. Toxicol.* **2015**, *8*, 55. https://doi.org/10.1515/intox-2015-0009

[4] J. A. Howard, L. David, F. Lux, O. Tillement, *J. Hazard. Mater.* **2024**, *478*, 135361. https://doi.org/10.1016/j.jhazmat.2024.135361

[5] World Health Organization, Guidelines for Drinking-water Quality, 4th ed., WHO Press, Geneva, 2017.

[6] U.S. Environmental Protection Agency, Lead and Copper Rule.

[7] M. Chalaris, D. A. Gkika, A. K. Tolkou, G. Z. Kyzas, *Environ. Sci. Pollut. Res.* **2023**, *30*, 119627–119653. https://doi.org/10.1007/s11356-023-30891-0

[8] K. S. More, J. P. Maree, M. Mahlangu, *Environ. Process.* **2025**, *12*, 15. https://doi.org/10.1007/s40710-025-00757-3

[9] E. L. Ungureanu, A. L. Mocanu, C. A. Stroe, C. M. Panciu, L. Berca, R. M. Sionel, G. Mustatea, *Sustainability* **2023**, *15*, 5999. https://doi.org/10.3390/su15075999
[10] H. Ibrahim, N. Sazali, W. N. W. Salleh, N. H. A. Ngadiman, N. A. Fadil, Z. Harun, *Biointerface Res. Appl. Chem.* **2022**, *12*, 5303–5323. https://doi.org/10.33263/BRIAC124.53035323
[11] M. M. Sabzehmeidani, S. Mahnaee, M. Ghaedi, H. Heidari, V. A. Roy, *Mater. Adv.* **2021**, *2*, 598–627. https://doi.org/10.1039/D0MA00087F
[12] M. Sulyman, J. Namieśnik, A. Gierak, *Pol. J. Environ. Stud.* **2017**, *26*, 479–510. https://doi.org/10.15244/pjoes/66769
[13] T. Fischer, A. Kretzschmar, V. Selmert, S. Jovanovic, H. Kungl, H. Tempel, R. A. Eichel, *RSC Adv.* **2024**, *14*, 3845–3856. https://doi.org/10.1039/D3RA07096D
[14] J. H. Kim, S. Y. Hwang, J. E. Park, G. B. Lee, H. Kim, S. Kim, B. U. Hong, *Carbon Lett.* **2019**, *29*, 281–287. https://doi.org/10.1007/s42823-019-00024-0
[15] G. Liu, Z. Dai, X. Liu, R. A. Dahlgren, J. Xu, *Carbon Res.* **2022**, *1*, 24. https://doi.org/10.1007/s44246-022-00025-1
[16] K. Malini, D. Selvakumar, N. S. Kumar, *J. CO_2 Util.* **2023**, *67*, 102318. https://doi.org/10.1016/j.jcou.2022.102318
[17] I. Langmuir, *J. Am. Chem. Soc.* **1918**, *40*, 1361–1403. https://doi.org/10.1021/ja02242a004
[18] H. Freundlich, *J. Phys. Chem.* **1906**, *57*, 385–470. https://doi.org/10.1515/zpch-1907-5723
[19] M. Temkin, V. Pyzhev, *Acta Physicochim. URSS*, **1940**, *12*, 217–222.
[20] S. Lagergren, *About the Theory of So-called Adsorption of Soluble Substances* **1898.**
[21] Y. S. Ho, G. McKay, *Process Biochem.* **1999**, *34*, 451–465. https://doi.org/10.1016/S0032-9592(98)00112-5
[22] W. J. Weber Jr., J. C. Morris, *J. Sanit. Eng. Div.* **1963**, *89*, 31–59. https://doi.org/10.1061/JSEDAI.0000430
[23] A. Jumasiah, T. G. Chuah, J. Gimbon, T. S. Y. Choong, I. Azni, *Desalination* **2005**, *186*, 57–64. https://doi.org/10.1016/j.desal.2005.05.015
[24] K. Vijayaraghavan, T. V. N. Padmesh, K. Palanivelu, M. Velan, *J. Hazard. Mater.* **2006**, *133*, 304–308. https://doi.org/10.1016/j.jhazmat.2005.10.016
[25] H. Marsh, F. R. Reinoso, Activated Carbon, Elsevier, **2006.** https://doi.org/10.1016/B978-0-08-044463-5.X5013-4
[26] R. C. Bansal, M. Goyal, Activated Carbon Adsorption, CRC Press, **2005**. https://doi.org/10.1201/9781420028812
[27] K. Y. Foo, B. H. Hameed, *Chem. Eng. J.* **2010**, *156*, 2–10. https://doi.org/10.1016/j.cej.2009.09.013
[28] Y. Xu, Y. Qu, Y. Yang, B. Qu, R. Shan, H. Yuan, Y. Sun, *Int. J. Mol. Sci.* **2022**, *23*, 14053. https://doi.org/10.3390/ijms232214053
[29] J. H. Kim, S. Y. Hwang, J. E. Park, G. B. Lee, H. Kim, S. Kim, B. U. Hong, *Carbon Lett.* **2019**, *29*, 281–287. https://doi.org/10.1007/s42823-019-00024-0
[30] D. Mohan, C. U. Pittman Jr., *J. Hazard. Mater.* **2007**, *142*, 1–53. https://doi.org/10.1016/j.jhazmat.2007.01.006
[31] M. Sevilla, R. Mokaya, *Energy Environ. Sci.* **2014**, *7*, 1250–1280. https://doi.org/10.1039/C3EE43525C
[32] M. C. Biesinger, *Surf. Interface Anal.* **2017**, *49*, 1325–1334. https://doi.org/10.1002/sia.6239
[33] J. Wang, X. Guo, *Chemosphere* **2020**, *258*, 127279. https://doi.org/10.1016/j.chemosphere.2020.127279
[34] S. M. Nasser, M. Abbas, M. Trari, *Prog. React. Kinet. Mech.* **2024**, *49*, 1–26.
[35] A. Pholosi, E. B. Naidoo, A. E. Ofomaja, *S. Afr. J. Chem. Eng.* **2020**, *32*, 39–55. https://doi.org/10.1016/j.sajce.2020.01.005
[36] F.-C. Wu, R.-L. Tseng, R.-S. Juang, *Chem. Eng. J.* **2009**, *153*, 1–8.
[37] W. Płaziński, W. Rudzinski, *J. Phys. Chem. C* **2009**, *113*, 12495–12501. https://doi.org/10.1021/jp902914z
[38] J. Wang, X. Guo, *Chemosphere* **2022**, *309*, 136732. https://doi.org/10.1016/j.chemosphere.2022.136732
[39] H. Zhang, J. Shao, S. Zhang, X. Zhang, H. Chen, *J. Hazard. Mater.* **2020**, *390*, 121349. https://doi.org/10.1016/j.jhazmat.2019.121349
[40] M. I. Inyang, B. Gao, Y. Yao, Y. Xue, A. Zimmerman, A. Mosa, P. Pullammanappallil, Y. S. Ok, X. Cao, *Crit. Rev. Environ. Sci. Technol.* **2016**, *46*, 406–433. https://doi.org/10.1080/10643389.2015.1096880
[41] L. Mouni, D. Merabet, A. Bouzaza, L. Belkhiri, *Desalination* **2011**, *276*, 148–153. https://doi.org/10.1016/j.desal.2011.03.038
[42] T. Van Thuan, B. T. P. Quynh, T. D. Nguyen, V. T. T. Ho, L. G. Bach, *Surf. Interfaces* **2017**, *6*, 209–217. https://doi.org/10.1016/j.surfin.2016.10.007
[43] D. Ramutshatsha-Makhwedzha, R. Mbaya, M. L. Mavhungu, *Materials* **2022**, *15*, 860. https://doi.org/10.3390/ma15030860
[44] T. K. Naiya, A. K. Bhattacharya, S. Mandal, S. K. Das, *J. Hazard. Mater.* **2009**, *163*, 1254–1264. https://doi.org/10.1016/j.jhazmat.2008.07.119
[45] S. Pap, J. Radonić, S. Trifunović, D. Adamović, I. Mihajlović, M. V. Miloradov, M. T. Sekulić, *J.* Environ. Manag **2016**, *184*, 297–306. https://doi.org/10.1016/j.jenvman.2016.09.089